

The Re-Emission Spectrum of Digital Hardware Subjected to EMI

Ian D. Flintoft, *Member, IEEE*, Andrew C. Marvin, *Member, IEEE*, Martin P. Robinson, Katharina Fischer, and Andrew J. Rowell

Abstract—The emission spectrum of digital hardware under the influence of external electromagnetic interference is shown to contain information about the interaction of the incident energy with the digital circuits in the system. The generation mechanism of the re-emission spectrum is reviewed, describing how nonlinear effects may be a precursor to the failure of the equipment under test. Measurements on a simple circuit are used to demonstrate how the characteristics of the re-emission spectrum may be correlated with changes to the digital waveform within the circuit. The technique is also applied to a piece of complex digital hardware where similar, though more subtle, effects can be measured. It is shown that the re-emission spectrum can be used to detect the interaction of the interference with the digital devices at a level well below that which is able to cause static failures in the circuits. The utility of the technique as a diagnostic tool for immunity testing of digital hardware, by identifying which subsystems are being affected by external interference, is also demonstrated.

Index Terms—Digital circuits, immunity, jitter, radio frequency interference, re-emission spectrum, timing delay.

I. INTRODUCTION

THE FAILURE of digital hardware in the presence of electromagnetic interference (EMI) is usually quite abrupt and typically requires the system to be reset or relock before normal operation can be continued. This is in contrast to analog systems which tend to show increasing effects as the EMI is increased and tend to recover spontaneously when the EMI is removed. Although the nature of digital equipment provides a degree of immunity to EMI, low levels of external interference can still cause problems.

Failures of digital hardware are generally classified as static or dynamic. Static failures occur at relatively high levels of interference, when the level of EMI induced in the digital signals is sufficient to cause false switching of gates in the circuit [1]. This occurs when the level of EMI induced on signal-bearing conductors becomes comparable to the difference in the switching thresholds of the logic. Static failure is characterized by the noise margin of the component devices in the circuit which defines the maximum amount the output of a device can

be perturbed without causing misinterpretation of the signal by a following compatible device. Dynamic failures are caused by changes in the propagation delay of a device, which leads to a violation of timing constraints such as hold times of flip-flops, and hence a failure of the circuit [2]–[4]. Changes in propagation delay can be the primary cause of failure at low levels of interference.

Static failures can occur even in the quiescent state of a digital system and are generally not strongly dependent on the state of the system (once interference reaches a level where false switching can occur, the state of the system is a secondary factor). Dynamic failures are, however, much more dependent on the state of the system, having a particular impact on the time variability of a system's susceptibility. The relative phase of the EMI and the logic transitions can lead to large changes in the failure rate on time scales of a few nanoseconds. Measurements have shown that synchronizing pulsed radio-frequency interference (RFI) with the digital signals in an equipment under test (EUT) can significantly increase the measured susceptibility of the EUT [5] and may provide a worst case estimate of the susceptibility. This type of failure has also been shown to be strongly dependent on the microcontroller architecture and software used by digital systems [6]. This makes it difficult to conduct repeatable immunity measurements on digital hardware, particular hardware with many different time scales in its cycles of operation. It would therefore be useful to have a measurement technique which could probe the extent to which external EMI is interacting with devices in a digital EUT at incident field levels below those which cause a repeatable observable failure. The perceived assessment of immunity is also unable to determine the effects of software error correction on the actual performance of digital systems in the presence of EMI and provides little indication of the risk of failure in different types of environment.

In this paper, we investigate whether the energy reradiated by a digital system when it is subject to external interference can be used to quantify the degree of interaction of the interference with the system, independently of any observed external functionality. A review of the generation mechanism of the emission spectrum is presented, indicating why it may be related to the susceptibility of digital hardware. The results of a series of measurements on a simple test board are presented and analyzed. We also correlate features in the reradiated spectrum of the illuminating energy with changes to the digital waveform in the circuit using optically coupled sensors on the test board. Finally, the technique is applied to a piece of complex digital hardware with several subsystems and failure modes.

Manuscript received May 24, 2002; revised June 4, 2003. This work was supported by the Radiocommunications Agency of the U.K. Department of Trade and Industry.

I. D. Flintoft, A. C. Marvin, and M. P. Robinson are with the Applied Electromagnetics Group, Department of Electronics, University of York, York YO10 5DD, U.K. (e-mail: idfl@ohm.york.ac.uk)

K. Fischer is with the Institut für Grundlagen der Elektrotechnik und Meßtechnik, University of Hanover, Hanover D-30167, Germany.

A. J. Rowell is with York EMC Services Ltd, University of York, York YO10 5DD, U.K.

Digital Object Identifier 10.1109/TEMC.2003.819058

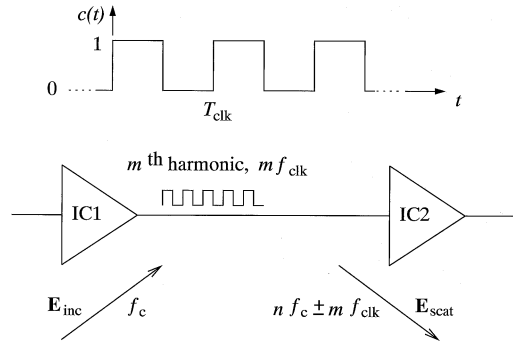


Fig. 1. Schematic illustration of the scattering of RFI by a digital system.

II. RE-EMISSION SPECTRUM

A. Generation Mechanism

The generation mechanism of the re-emission spectrum can be demonstrated using the simple circuit in Fig. 1, which consists of a single transmission line (PCB track) between two integrated circuits (ICs). An external sinusoidal electromagnetic field \mathbf{E}_{inc} of angular frequency ω_c illuminates the transmission line giving rise to RF voltages and currents in the conductors. We will assume that the frequency of the RF radiation is much greater than the clock frequency f_{clk} of the digital waveform between the two ICs and for simplicity take the waveform to be a pure square-wave clock signal $c(t)$ with period T_{clk} as shown in Fig. 1.

Consider the situation just after the digital signal goes high (H). The output impedance of IC1 in the high state is Z_{1H} and the input impedance of IC2 is Z_{2H} . After a short transient period the RF energy coupled to the transmission line will reach a steady state, with a corresponding voltage and current distribution which depends on the impedances Z_{1H} and Z_{2H} . From the assumption $\omega_c \gg \omega_{\text{clk}}$, this transient lasts for only a small fraction of the clock period. The current on the line will give rise to a reradiated electromagnetic field \mathbf{E}_{scat} , whose amplitude and phase also depend on the impedances Z_{1H} and Z_{2H} . As the digital signal switches to the low (L) state, there will be another short transient after which a new RF steady state will be reached which depends on the, generally different, impedances Z_{1L} and Z_{2L} of the ICs low state. The amplitude and phase of the reradiated field will therefore also change as the circuit switches.

We can therefore write the reradiated field at some observation point \mathbf{r} as

$$\begin{aligned} \mathbf{E}_{\text{scat}}(\mathbf{r}, t) = & \mathbf{E}_H(\mathbf{r})c(t) \cos(\omega_c t + \phi_H(\mathbf{r})) \\ & + \mathbf{E}_L(\mathbf{r}) (1 - c(t)) \cos(\omega_c t + \phi_H(\mathbf{r})) \end{aligned} \quad (1)$$

where $\mathbf{E}_{H,L}$ and $\phi_{H,L}$ are the amplitude and phase in the high and low states, respectively, and ω_c is the angular frequency of the incident field. $\mathbf{E}_{H,L}$ and $\phi_{H,L}$ will be functions of the circuit geometry, observation position, incident field strength, and other parameters. This relation explicitly demonstrates the two-state nature of the reradiated electromagnetic field, which is a signature of the interaction between the incident field and the digital circuit. In the frequency domain, the spectrum of the reradiated field given by (1) can be written as

$$\mathbf{E}_{\text{scat}}(\mathbf{r}, \omega) = \mathbf{E}_{\text{carrier}}(\mathbf{r}, \omega) + \mathbf{E}_{\text{mod}}(\mathbf{r}, \omega) \quad (2)$$

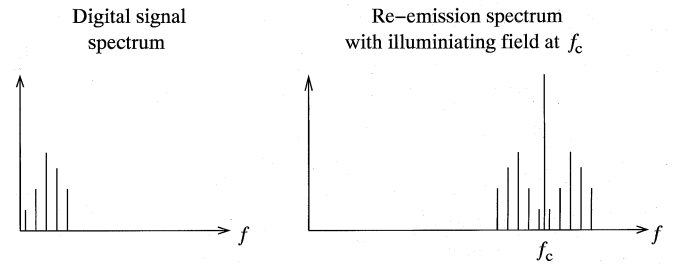


Fig. 2. Illustration of the re-emission spectrum showing the harmonics of the digital signal mirrored either side of the incident carrier frequency.

where $\mathbf{E}_{\text{carrier}}(\mathbf{r}, \omega)$ is the scattered carrier term and $\mathbf{E}_{\text{mod}}(\mathbf{r}, \omega)$ is the frequency shifted cross-modulation component, given by

$$\mathbf{E}_{\text{mod}}(\mathbf{r}, \omega) = \mathbf{A}_+ C(\omega + \omega_c) + \mathbf{A}_- C(\omega - \omega_c) \quad (3)$$

where

$$\mathbf{A}_{\pm} = \frac{1}{2} \{ \mathbf{E}_H e^{\mp j \phi_H} - \mathbf{E}_L e^{\mp j \phi_L} \} \quad (4)$$

and

$$C(\omega) = \sum_{m=-\infty}^{m=+\infty} \frac{2}{m} e^{-j m \pi D} \sin(m \pi D) \delta\left(\omega - \frac{2 \pi m}{T_{\text{clk}}}\right) \quad (5)$$

is the spectrum of the digital signal, now generalized to allow for a duty cycle D , which need not be 0.5. The spectrum therefore consists of the incident field phase and amplitude modulated by the clock signal in the circuit as illustrated in Fig. 2. The characteristic spectrum of the digital circuit that is subjected to the external interference is therefore manifested in the re-emission spectrum as cross-modulation sidebands. This suggests the possibility of both identifying that a digital circuit is suffering interference and also quantifying the effect, before any functional misbehavior of the circuit occurs. In practice, the coupling path of the reradiated field out of the EUT will also shape the form of the re-emission spectrum, and hence, the envelope of the modulation spectrum will be different to that of $c(t)$. However, the cross-modulation products (CMPs) will still occur at frequencies given by

$$f_{\text{CMP}} = f_c \pm m f_{\text{clk}} \quad (6)$$

where m is a positive integer, allowing the spectrum to be associated with the interaction of the incident field with a digital circuit clocked at frequency f_{clk} . For an unperturbed square-wave clock signal, only CMPs with odd values of m will appear in the re-emissions spectrum. Since the spectrum of the digital waveform is correlated with the pure emission spectrum of the EUT the re-emission spectrum will also be strongly correlated with the low frequency emission spectrum of the circuit. However, the amplitudes of the spectral components in both spectra will be modified by different transfer functions of the coupling paths taken by the radiation out of the equipment.

The theory in [7] shows how to predict the magnitude of these CMPs around the incident frequency for a simple circuit. This correlation of the shifted pure emission spectrum and reradiated spectrum shows that the RFI has penetrated into the parts of

the system characterized by the spectral content of the emission spectrum.

B. Nonlinear Effects

The amplitudes of the CMPs in the re-emission spectrum cannot be used directly to quantify whether or not the degree of interaction between a circuit and RFI is likely to cause disruption. Indeed, CMPs can be visible even at quite low levels of RFI. In order to obtain susceptibility information about the EUT, we must consider the linearity of the re-emission with increasing incident field strengths. When the level of the inference signal induced on the transmission line is low, the amplitude of the reradiated CMPs rises linearly with the incident field strength, as shown by (3).

However, once the level of interference is sufficient to cause the induced interference voltage on the transmission line to move into the nonlinear switching regime of the digital devices the interaction will start to become nonlinear [8]. This will give rise to two important effects. First, the amplitude of the CMPs will no longer be linearly related to the incident field strength, but will depend on the switching profile of the digital devices. Second, the nonlinear reflections from the devices will give rise to intermodulation products between the incident field and the digital signal. In particular, harmonics of the incident frequency, f_c , will be generated which will also become cross-modulated by the digital waveform. This will result in the reproduction of the distorted digital spectrum of the digital equipment around harmonics of the incident frequency, leading to higher order CMPs at frequencies

$$f_{\text{CMP}} = n f_c \pm m f_{\text{clk}} \quad (7)$$

where $n > 1$. Both these effects are indicators that the interference in the circuit has reached a level at which it is beginning to disturb the operation of the circuit. It is expected that the onset of these effects will coincide with variations in timing, and other interference phenomena in the digital circuits since these are caused by the same disturbances as the nonlinear re-emissions.

C. Complex EUTs

For complex EUTs with many subsystems, the cross-modulation of the RFI can occur in numerous circuits with different clock frequencies. The re-emission spectrum may then contain CMPs related to more than one subsystem in the EUT. In (3), the effect of the transfer functions of the incident field into the EUT and the scattered field out of the EUT was not considered. For real EUTs, both these effects will have an impact on the re-emissions. The parameters \mathbf{A}_{\pm} corresponding to the scattering from a *single* circuit will, in fact, take the form

$$\mathbf{A}_{\pm}(\mathbf{r}, \omega) \sim \sum_{\substack{\text{paths} \\ \text{out}, o}} \left[\hat{T}_o^{\text{out}}(\mathbf{r}, \omega) \left\{ \sum_{\substack{\text{paths} \\ \text{in}, i}} \hat{T}_i^{\text{in}}(\mathbf{r}, \omega_c) \right\} \right] \mathbf{E}_{\text{inc}}(\omega_c). \quad (8)$$

The tensor operator \hat{T}_i^{in} is the transfer function of incident energy into the EUT along coupling path i and \hat{T}_o^{out} is the transfer function out of the EUT along path o . Note that the terms in this equation are not likely to be known quantitatively. The term in

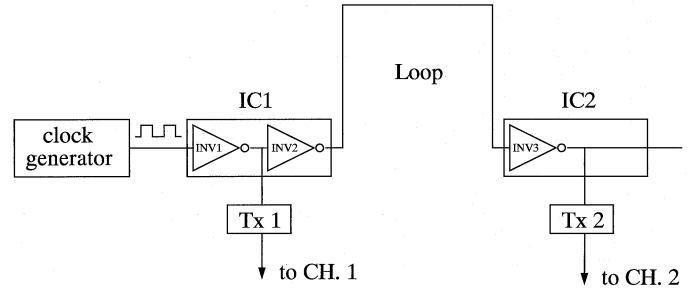


Fig. 3. Schematic circuit diagram of the test board.

{ } braces represents the coupling of energy from the incident field into the circuit in question via a number of different coupling paths at the illuminating frequency ω_c . This term therefore constitutes the key information about the immunity of the circuit since it determines the interference energy incident on devices in the circuit. The measured re-emission spectrum, however, also depends on how the cross-modulated energy at frequencies $n\omega_c \pm m\omega_{\text{clk}}$ generated in the circuit is propagated out of the system. Since this occurs at different frequencies to the ingress, it will, in general, occur via different coupling paths with different properties. This will cause distortion of the reradiated spectrum and thus alter the relative amplitudes and phases of the CMPs from those predicted by the simple model described in (3).

Ultimately, the utility of the technique will depend upon to what extent the coupling path out of the EUT distorts the susceptibility indicators we wish to measure. The onset of nonlinear behavior, for example, should not be affected and may therefore be a device independent indication that the RFI is potentially strong enough to cause failures.

III. OPTICALLY COUPLED TEST BOARD AND DIGITAL TELEVISION SATELLITE RECEIVER

The circuit diagram of the test board constructed for the measurements is shown in Fig. 3. The board consisted of a clock oscillator module driving three consecutive inverters housed in two separate IC packages. The board was designed to maximize the coupling of external RFI to the track between the second and third inverters and to minimize the coupling elsewhere in the circuit. This was achieved by using a large loop of track between the second and third inverter and very short tracks lengths between the other components. The board was single sided without a ground plane and powered by batteries. Sockets were used for both the oscillator and inverter modules so that different clock frequencies and logic device families could be investigated. For the measurement results presented here, 74LS inverter packages were used.

To allow the measurement of timing variations and jitter induced in the circuit, two TTL-compatible diode modules were connected between the first and second inverters and after the last inverter. These allowed optical links, with a bandwidth of about 10 MHz, to be used to monitor the digital waveforms in the circuit.

A piece of digital equipment representative of modern hardware was also subjected to the re-emission technique. The

TABLE I
DIGITAL TELEVISION SATELLITE RECEIVER
SUBSYSTEMS

Functional Subsystem	Clock Frequency (MHz)	Label
Modem	8.38861	m
Smart card reader	14.7456	s
Decoder and flash memory	27.0000	d
Processor operation	29.4912	p

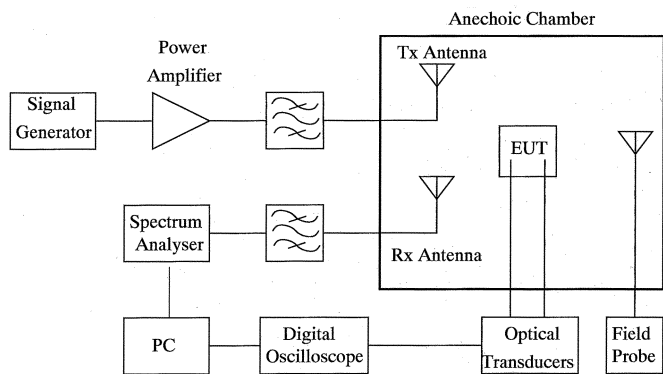


Fig. 4. Experimental configuration used for re-emission spectrum measurements.

equipment used was a digital television satellite receiver; a relatively complex EUT with several different digital subsystems. Table I summarizes the four main subsystems identified in the satellite receiver and their associated clock frequencies. Note that the clock frequency of the processor is exactly twice that of the smart card reader.

IV. MEASUREMENT METHODOLOGY

Measurements were conducted in a fully anechoic chamber and a gigahertz transverse electromagnetic (GTEM) cell, using standard EMC test equipment. The EUT was illuminated using a signal generator and power amplifier via a suitable transducer for field generation. For measurements in an anechoic chamber, as shown in Fig. 4, the transducer was a broadband EMC antenna while for measurements in a GTEM cell the septum of the cell was used. The scattered electromagnetic field was probed using a second transducer which was either another antenna or the same transducer used for field generation if suitable splitting and combining networks could be employed. A spectrum analyzer or EMI receiver was used to measure the scattered field. Power or field monitoring equipment were also used to give an indication of the applied field and to ensure linearity when several test levels were used.

In a practical measurement environment, the cross-modulated field will be only one component of the total field that is measured in a receiver. In general, the total field consists of four terms

$$\mathbf{E}_{\text{tot}} = \mathbf{E}_{\text{direct}} + \mathbf{E}_{\text{passive}} + \mathbf{E}_{\text{scat}} + \mathbf{E}_{\text{rad}} \quad (9)$$

where $\mathbf{E}_{\text{direct}}$ is the direct coupling between the transmission and reception antennas, $\mathbf{E}_{\text{passive}}$ is the unmodulated portion of

the field, which has scattered from passive structures in the EUT, \mathbf{E}_{scat} is the scattered field that has interacted with digital circuits, and \mathbf{E}_{rad} is the active radiated emissions of the EUT. From (2), \mathbf{E}_{scat} contains the scattered carrier term and the modulation sidebands \mathbf{E}_{mod} . For real EUTs, \mathbf{E}_{scat} will have a complex spectrum since many different circuits may be interfered with and the scattering will be distributed in nature.

The presence of a strong directly coupled field limits the amount of power that can be injected into the test circuit in order to prevent overload and damage to the spectrum analyzer or receiver. It is also essential that any nonlinearities in the measurement system be minimized in order to prevent any misinterpretation of the results. A bandpass filter was therefore used to block any harmonics of the incident frequency generated in the amplifier and signal generator from illuminating the EUT. Ideally, a tunable bandstop filter would also have been used to block the directly coupled illuminating field from entering the receiver system. This would protect the spectrum analyzer and reduce the potential for nonlinear interactions in the front end of the receiver due to the strong directly coupled incident energy. Practically the same effect was achieved using a second bandpass filter with high selectivity to observe parts of the re-emission spectrum containing features of interest. When the EMI receiver was employed, its tracking filter selectivity was used to attenuate the directly coupled and unmodulated components of the field. In either case, the filter selectivity limits how close to the illuminating frequency the re-emissions can be measured. Cross polarizing the transmitting and receiving antenna also provided some isolation between the antennas at the illuminating carrier frequency in an anechoic chamber. Note that the scattered spectrum from an EUT is generally randomized in polarization. The calibration of the incident field was made with the EUT removed from the chamber and the electric field probe placed in the position of the board.

For the test board measurements, a 500-MHz digital oscilloscope was used to monitor the delay between the logic transitions at the output of the second and third inverters. The oscilloscope was triggered using the leading edge of the waveform at the output of the second inverter. Timing variations on the leading edge of the output from the third inverter could then be estimated using the infinite persistence feature of the oscilloscope. The relative delay over the two optical links was calibrated out of the measured timings. The test board was illuminated with a sinusoidal field of increasing field strength at a number of frequencies. In each case, the level of CMPs in the re-emission spectrum near the illuminating frequency, and also near twice the illuminating frequency were measured, along with the maximum jitter and any variation in switching times of both the leading and trailing edges of the output of the last inverter.

All tests on the digital television satellite receiver were performed in a GTEM cell with the GTEM used for field illumination. A small loop was used as the sensing antenna and placed at various positions within the satellite receiver box. The satellite receiver was fed by an off-air signal and tuned into a free-to-air channel displayed on an external television monitor. It was exposed to RFI across a broad frequency range to identify susceptible frequencies. Two such frequencies where the receiver

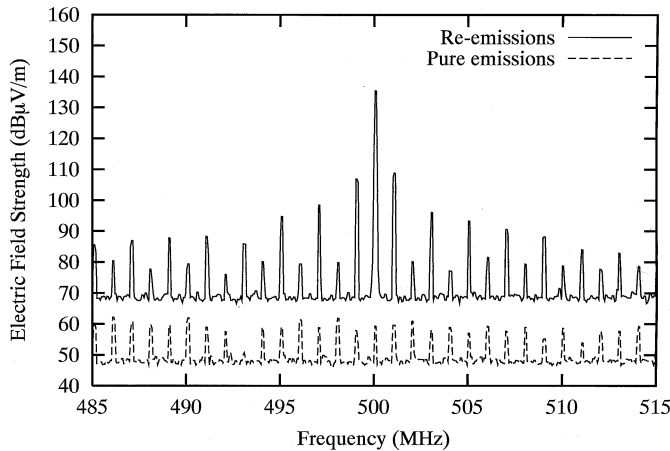


Fig. 5. Comparison of the pure emission spectrum and re-emission spectrum of the test board with a 6-V/m illuminating field at $f_c = 500$ MHz.

exhibited failures (275 and 840 MHz), were selected and the results of the investigations at these frequencies are presented.

V. RESULTS: RE-EMISSION SPECTRA OF TEST BOARD

A typical re-emission spectrum obtained from the measurements is shown in Fig. 5, compared to the pure emission spectrum with no incident field. The clock frequency is 1 MHz and the illuminating frequency 500 MHz. In this case, the frequency components from the pure emission spectrum coincide with the CMPs in the re-emission spectrum, so the spectrum obtained is a superposition of both the pure emissions and the re-emissions. However, this effect can be neglected, because the pure emissions are at a much lower level than the re-emissions. Note that noise from the transmitting apparatus and extra attenuation in the receiving equipment when the illuminating field is switched on are responsible for the two different noise floor levels in Fig. 5.

Fig. 6 shows the general behavior of the re-emission spectrum with increasing incident field strength. While initially only the incident carrier and the onset of two CMPs at 500 ± 1 MHz are observable, more CMPs are generated at higher incident field strengths. The choice of a square-wave clock signal for the test board means that CMPs due to even harmonics of the clock are at a low level in the unperturbed circuit; even CMPs can then be used as a diagnostic for the penetration of interference energy into the circuit. The detailed behavior of the re-emission spectrum for a number of measurements is discussed in the following subsections.

A. 500-MHz Illuminating Field

The test board was initially illuminated with a 500-MHz sinusoidal field. The graphs in Fig. 7 show how the received electric field strength of the observed CMPs changed as the incident field was varied from 0 to 24 V/m. In this measurement, the test board failed at an incident field strength of about 20.5 V/m. At this level of interference, the last inverter stopped switching. The trigger signal output from the first inverter, however, was not obviously affected by the EMI.

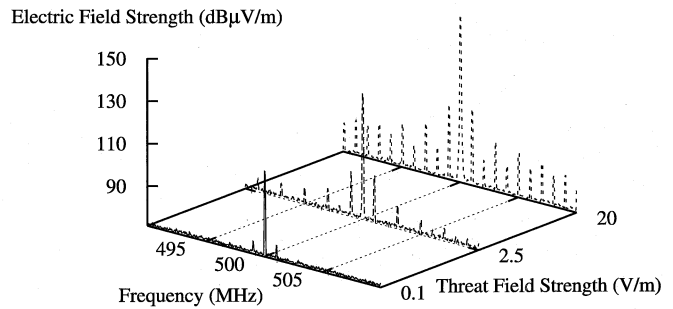


Fig. 6. Variation of the re-emission spectrum of the test board around the illuminating frequency $f_c = 500$ MHz with increasing illuminating field strength.

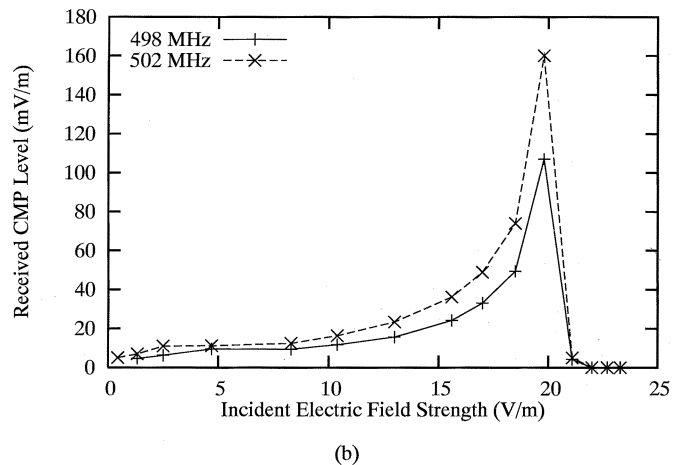
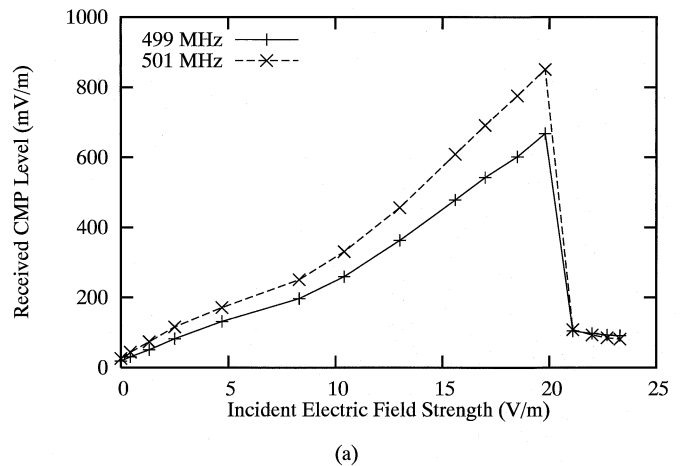
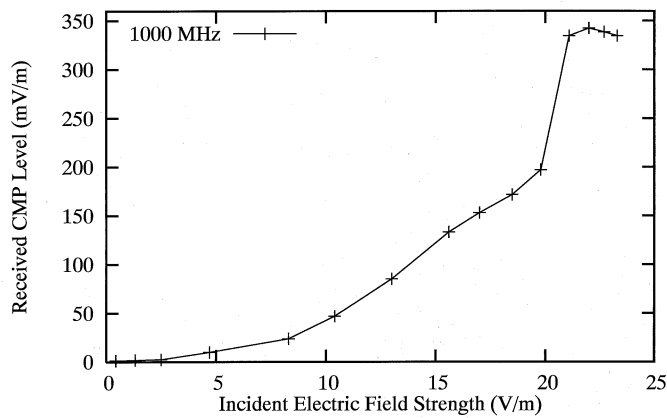
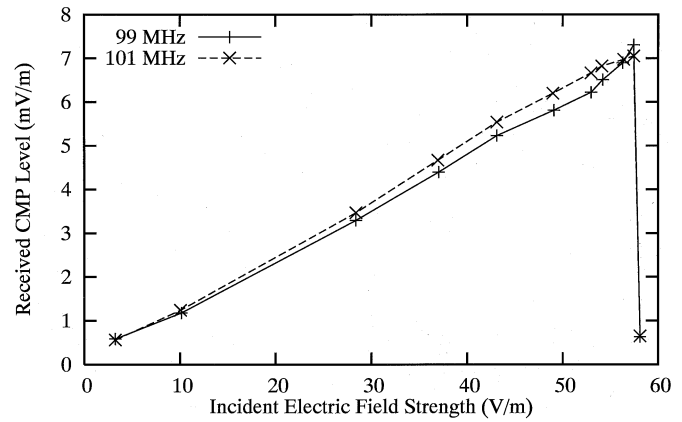


Fig. 7. Variation of the level of first order ($n = 1$) CMPs from the test board with incident field strength for $f_c = 500$ MHz. (a) $m = \pm 1$. (b) $m = \pm 2$.

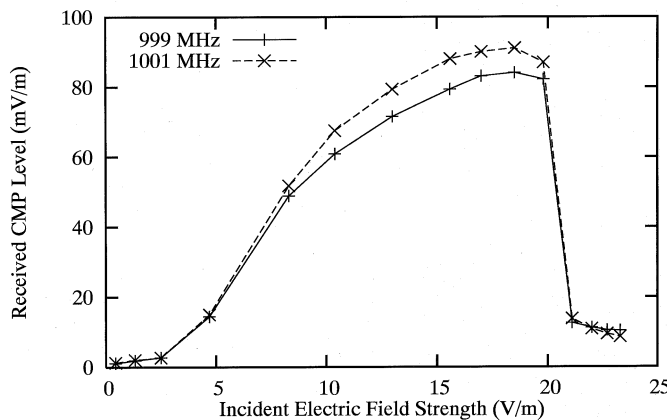
Fig. 7(a) shows the variation of the CMPs at 499 and 501 MHz, which are representative of the behavior of all the measured CMPs corresponding to odd harmonics, i.e., an approximately linear rise until the failure level is approached; there is an inflection in the curve at 9 V/m, about 7 dB below the failure level. When the board fails the odd CMPs decrease to a much lower level, however, even after failure the odd harmonics remain above the noise floor, indicating that the interference is still interacting with some switching devices in the circuit.



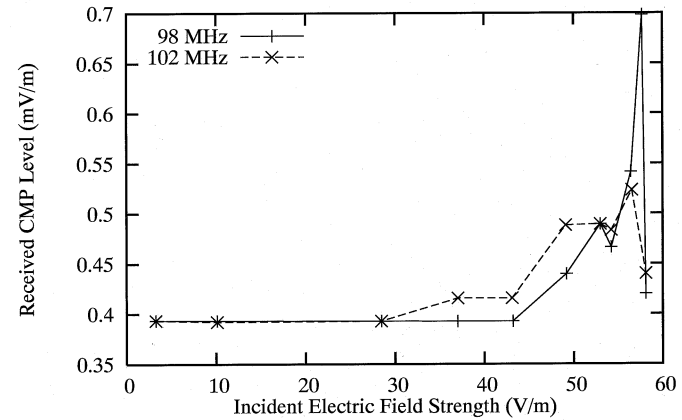
(a)



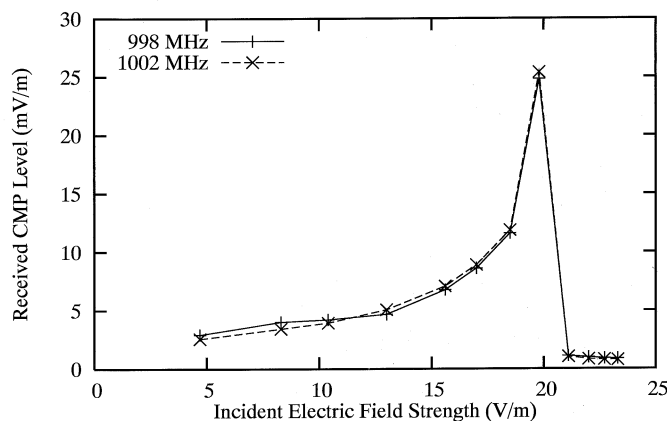
(a)



(b)



(b)



(c)

Fig. 8. Variation of the level of second order ($n = 2$) CMPs from the test board with incident field strength for $f_c = 500$ MHz: (a) $m = 0$; (b) $m = \pm 1$; (c) $m = \pm 2$.

The levels of the even CMPs, for example, those at 498 and 502 MHz shown in Fig. 7(b), initially do not change significantly and then rise rapidly beyond 15 V/m when the EUT approaches failure. When the board stops switching, these frequency components disappear completely from the re-emission spectrum.

CMPs could also be observed around the first harmonic of the incident frequency. The component at 1000 MHz, shown in Fig. 8(a), rises continuously until the point at which the EUT fails. This frequency component is generated by the nonlinear

Fig. 9. Variation of the level of first order ($n = 1$) CMPs from the test board with incident field strength for $f_c = 100$ MHz. (a) $m = \pm 1$. (b) $m = \pm 2$.

characteristics of the EUTs active devices when the illuminating energy is propagated and reflected within the circuit. Therefore, it is dependent on the state of the system, which is influenced by both the clock and the interfering signal.

The CMPs at 999 and 1001 MHz shown in Fig. 8(b) have a similar behavior to the corresponding CMPs around the carrier itself at 499 and 501 MHz. However, close to failure, the CMPs with $n = 2$ have a distinctly “flatter” behavior than those for $n = 1$. This effect is caused by the nonlinear shape of the 1000-MHz component, which also influences the level of the surrounding CMPs due to the generation mechanism of the modulated scattering. The shapes of the graphs for the CMPs at 998 and 1002 MHz, shown in Fig. 8(c), are very similar to the shapes measured at 498 and 502 MHz, but at about a 20 dB lower level. Note that different levels of cross-modulation products corresponding to the same harmonic of f_{clk} are due to the nonconstant transfer function of the EUT.

B. 100 MHz Illuminating Field

The test board was also illuminated with a lower frequency incident field at 100 MHz. Fig. 9 shows the measured levels of the CMPs at 98, 99, 101, and 102 MHz, respectively. The CMPs corresponding to the odd harmonics show an almost linear slope with a slight flattening at the point of failure at an incident field strength of 57 V/m. Note that it was only just possible to cause

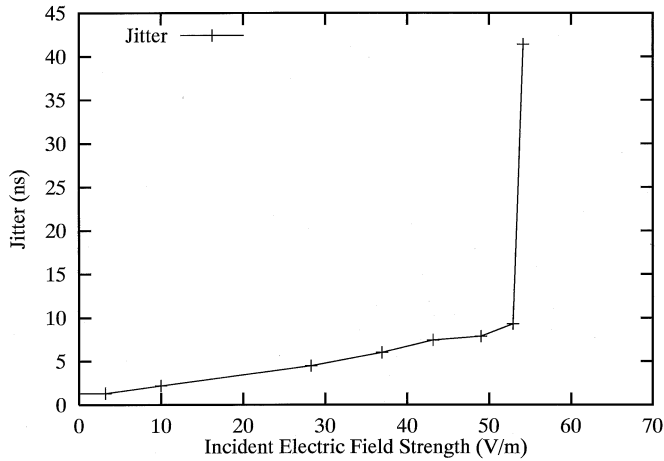


Fig. 10. Variation of timing jitter in the test board with the incident field strength using 74LS logic for $f_c = 100$ MHz.

failure at this frequency with the equipment available. As already observed during the investigations with the 500-MHz illuminating field, the even harmonics increase rapidly toward failure and then fall to much lower levels afterwards.

VI. RESULTS: CORRELATION OF RE-EMISSIONS WITH CHANGES TO DIGITAL SIGNALS IN TEST BOARD

Two different types of change in the digital signal in the circuit were observed during the measurements on the test board:

- 1) timing jitter on the rising and falling edges of the square wave;
- 2) change in the duty cycle of the digital signal.

Interestingly, we observed two cases in which the failure was accompanied predominantly by only one of these effects allowing them to be analyzed independently.

A. Changes in Timing Jitter

Fig. 10 shows the measured timing jitter on the test board subjected to the 100-MHz incident field, corresponding to the re-emission spectrum results in Fig. 9. The timing jitter initially rises approximately linearly with the incident field strength and then suddenly increases rapidly close to failure. The mean duty cycle of the clock signal was almost unaffected by the increasing incident field level in this experiment. This is typical of the expected behavior for interference which is within the passband of the devices [2].

From (5), the magnitude of the m th Fourier spectral component of a rectangular waveform of amplitude A and duty cycle D is given by

$$|c_m(D)| = \frac{A}{\pi m} \sin(m\pi D) \quad (10)$$

where $m = 1$ is the fundamental frequency, $m = 2$ the first harmonic, etc. Hence, the ratio of the CMPs with $m = 2$ and $m = 1$ can be estimated as

$$\left| \frac{c_2(D)}{c_1(D)} \right| = \cos(\pi D) \quad (11)$$

assuming that the re-emission spectrum is not significantly distorted by the frequency-dependent transfer function of the test

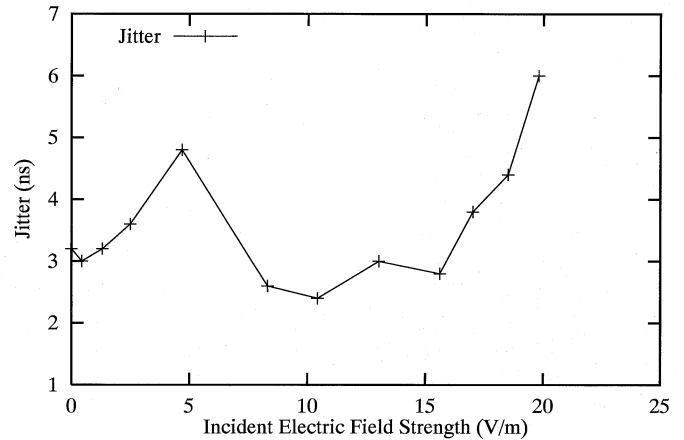


Fig. 11. Variation of timing jitter in the test board with the incident field strength for $f_c = 500$ MHz.

board over the frequency range $f_c - 2f_{\text{clk}} < f < f_c + 2f_{\text{clk}}$. If the mean duty cycle remains unaffected by the RFI, this simple model would suggest that CMPs with even m , such as those shown in Fig. 9(b) should not be observed at a significant level.

However, timing jitter is a statistical spreading in the transition times of the digital signals. For an unmodulated illuminating field, the timing jitter has the highest probabilities near the extremes of its distribution. Hence, if the maximum jitter is about 40 ns for a 1-MHz clock frequency, as in Fig. 10, the duty cycle will mainly take on values close to 0.46 or 0.54, respectively, and so generate even harmonics even though the mean duty cycle is 0.5. From (11), these duty cycles lead to a ratio of $|c_2/c_1|$ of about 0.12, which is consistent with the relative levels of odd and even CMPs measured in Fig. 9(b). The statistical distribution of the timing jitter is also asymmetric which would also tend to generate even CMPs in the re-emission spectrum [9].

B. Changes in Duty Cycle

A different behavior was observed when the EUT was illuminated with a 500-MHz field. Figs. 11 and 12 show the measured timing jitter and mean duty cycle, respectively, as a function of the illuminating field strength. In contrast to the previous case with an illuminating frequency of 100 MHz, the jitter does not rise systematically toward failure when the board is subjected to the 500-MHz incident field. Furthermore, the maximum timing jitter of about 6 ns before the board stops working is significantly lower than the corresponding jitter under the influence of the 100-MHz interference. This may be attributed to the fact that the interference is outside the passband of the device. The duty cycle in case of the 500-MHz incident field, however, was found to vary strongly with the level of interference, as can be seen in Fig. 12. While the trigger signal from the first inverter remained almost unaffected, the duty cycle of the output voltage behind the last inverter showed a strong increase toward failure.

The rise of the even harmonics in the re-emission spectrum [see Fig. 7(b)] can be explained by the shift in duty cycle away from 0.5 using relation (10). Fig. 13 shows the theoretical increase of the even harmonics due to the change of duty cycle plotted in Fig. 12 that was computed using (10). The agreement

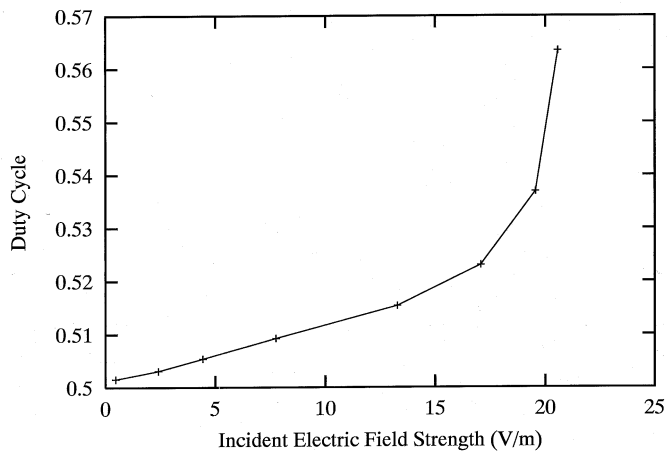


Fig. 12. Variation of duty cycle in the test board with the incident field strength for $f_c = 500$ MHz.

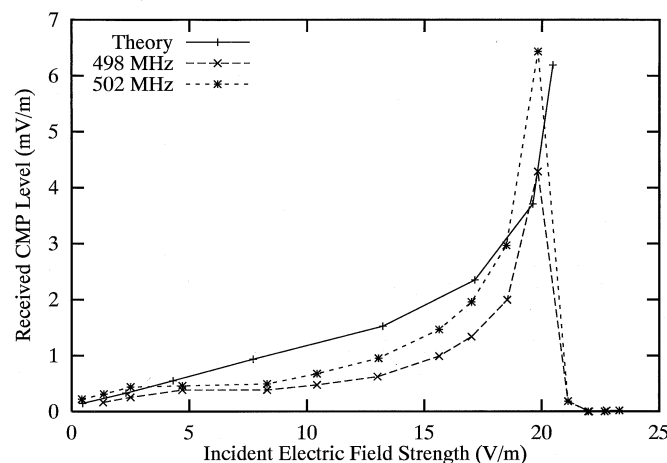


Fig. 13. Theoretical and measured increase in CMPs from the test board for $f_{inc} \pm f_{clk}$.

of the theory with the measurement results shows that there is a correlation between the duty cycle variation and the corresponding strong increase of the even harmonics in the re-emission spectrum that was observed when the EUT was subjected to the 500-MHz illuminating field.

VII. RESULTS: DIGITAL TELEVISION SATELLITE RECEIVER

Fig. 14 is an example of an emission spectrum from the satellite receiver for an incident field at 275 MHz. The solid trace shows the measured emissions profile without an applied field and the dashed trace corresponds to a field strength of approximately 45 V/m. Re-radiated cross-modulation products (marked \diamond) can clearly be seen to emerge as the field strength increases. The general increase in broadband noise is due to the fact that the amplifier output was not limited by a band pass filter in this case. The CMP frequencies measured are all associated with on-board oscillators operating at 14.7456 or 29.4912 MHz. The frequencies of the strongest CMPs are given in Table II, which also indicates the corresponding value of m in (7) for each subsystem clock frequency in Table I.

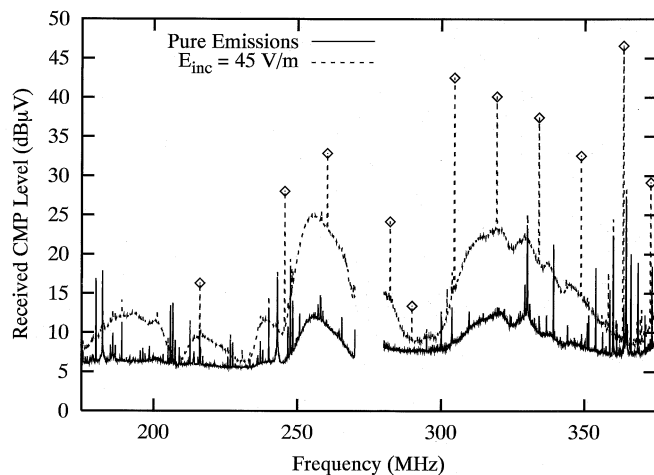


Fig. 14. Re-emission spectrum of the satellite receiver with a 45-V/m incident field (dashed line) at 275 MHz compared to pure emission spectrum (solid line).

TABLE II
FREQUENCIES OF SOME OF THE STRONGEST CMPs FOR THE SATELLITE RECEIVER WITH A 275 MHz ILLUMINATING FIELD

CMP Frequency (MHz)	m for each subsystem		
	m	s	p
245.50	-	-2	-1
260.26	-	-1	-
304.54	-	+2	+1
319.24	-	+3	-
334.00	+7	+4	+2
348.76	-	+5	-
363.46	-	+6	+3

A graph of the reradiated emission against field strength for the 275 MHz incident field is shown in Fig. 15. At this interfering frequency, the first malfunction observed was failure to respond to the remote control (Fail 1) at 153 dB μ V/m (\sim 45 V/m) followed by a rapid on-screen search through all available channels (Fail 2) at 157 dB μ V/m (\sim 70 V/m) and random channel selection at 160 dB μ V/m (\sim 100 V/m).

The appearance of nonlinear behavior in the re-emissions associated with the 29.4912- and 14.7456-MHz clocks suggests that the main processor and smart card decoder subsystems were being affected by the interference. Investigations were performed using a small loop antenna to inject interference at various points within the unit. The most sensitive area was indeed found to be in the region of the circuits associated with these oscillators.

Fig. 16 shows the development of the reradiated emissions profile at an illuminating frequency of 840 MHz as the applied field strength is increased up to approximately 160 V/m. The strongest CMPs and associated values of m are given in Table III. The first malfunction noted was again failure of the EUT to respond to the remote control (Fail 1) at an incident field strength of 153 dB μ V/m (\sim 45 V/m), followed by the freezing of the picture (Fail 2) at 156 dB μ V/m (\sim 65 V/m) and then the display of a channel information banner at the maximum applied amplifier input of 160 dB μ V/m (\sim 100 V/m).

This is a different failure mode to that observed with the 275-MHz illuminating frequency. When the resultant emissions against interference level curves are examined, it is

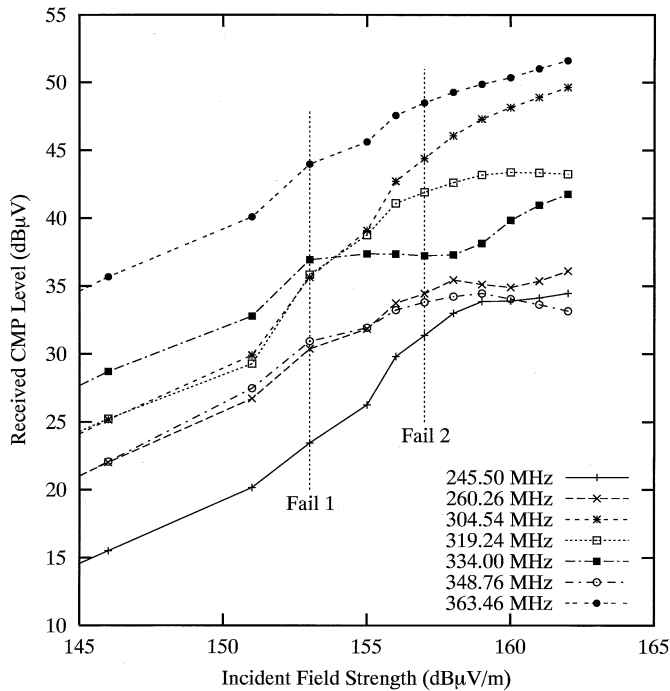


Fig. 15. Level of CMPs versus incident field strength for satellite receiver with 275-MHz incident field.

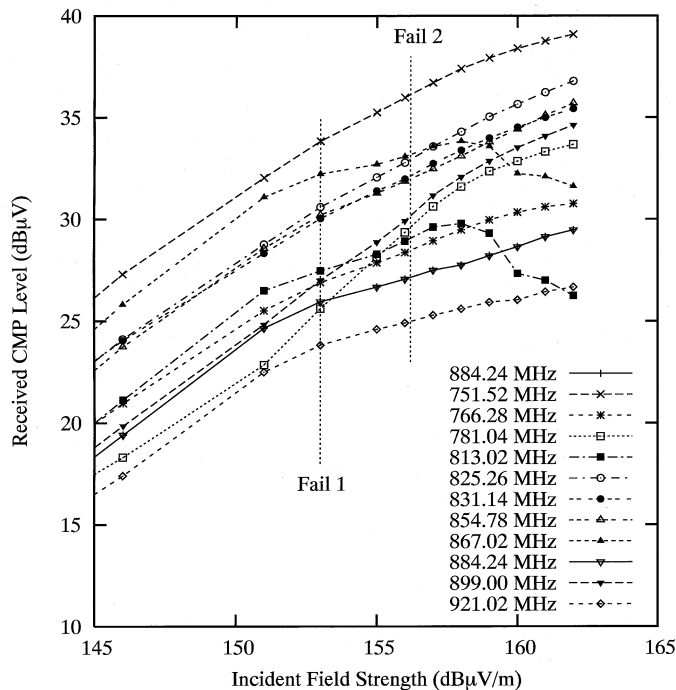


Fig. 16. Level of CMPs versus incident field strength for satellite receiver with 840-MHz incident field.

observed that emissions are present which are associated with the 14.7456-MHz oscillator, the 27.0-MHz oscillator, and possibly the 29.4912-MHz oscillator. The curves for 813.02 and 867.02 MHz show significant changes in gradient at interference levels approaching and exceeding EUT malfunction, beginning at 5 dB before malfunction. This suggests that although the interfering energy is penetrating several circuits

TABLE III
FREQUENCIES OF SOME OF THE STRONGEST CMPs FOR THE SATELLITE RECEIVER WITH A 840-MHz ILLUMINATING FIELD

CMP Frequency (MHz)	m for each subsystem			
	m	s	d	p
751.52	-	-6	-	-3
766.28	-	-5	-	-
781.04	-7	-4	-	-2
813.02	-	-	-1	-
825.26	-	-1	-	-
831.14	-1	-	-	-
854.78	-	+1	-	-
867.02	-	-	+1	-
884.24	-	+3	-	-
899.00	+7	+4	-	+2
921.02	-	-	+3	-

or subsystems, the circuitry most affected by the interference is that associated with the 27.0-MHz oscillator (the decoder and flash memory). Localized injection of interference using the small loop showed that the most sensitive area in the EUT at this frequency was the area around the 27.0-MHz oscillator, supporting this supposition.

VIII. CONCLUSION

The mechanism responsible for the generation of cross-modulation products in the re-emission spectrum of digital systems is closely related to that which causes static failures and timing jitter in the disturbed digital circuits, i.e., excursions into the switching region of the devices leading to nonlinear scattering. This suggests the possibility of using the re-emission spectrum to probe the susceptibility of a digital system.

Measurement results for a simple test board have demonstrated that the re-emission spectrum can be observed and that nonlinearity in the behavior of CMPs may be a precursor to failure of the system. The failure point of the circuit is clearly visible in the behavior of the re-emission spectrum about both the incident frequency and the first harmonic of the incident frequency.

By monitoring the digital waveforms on the board using optical links a correlation was established between the re-emission spectrum and changes in the digital waveform in the circuit. The variations observed, both the change of duty cycle and the rising timing jitter, were found to be correlated to a strong increase of the CMPs corresponding to the even harmonics of the clock signal. Both these correlations have been justified theoretically. In each case, the eventual static failure of the test boards was immediately preceded by strongly nonlinear behavior of the CMPs in the re-emission spectrum.

The re-emission spectrum of a piece of complex digital hardware could also be correlated with the immunity of the equipment. Specifically, nonlinear behavior in the cross-modulation products from a digital television satellite receiver was observed as the incident field strength approached that required to cause equipment failure. The rapid increase in even harmonics associated with the simple test boards was not seen in the complex EUT, presumably due to the large background spectrum from devices which continue to operate normally and the lack of pure square-wave digital waveforms. A more subtle, but nevertheless

observable change in emissions profile could be detected before failure. Examination of the results obtained suggests that the linearity of the reradiated emissions begins to be lost at field strengths approximately 5 dB below the level required to cause the equipment to fail.

Using knowledge of the internal sub-systems within the satellite receiver, in particular the clock oscillator frequencies, it was possible to identify from the re-emission spectrum which system in the receiver was failing at different interfering frequencies. The identification was verified by locally injecting interference into the subsystems concerned and checking that the failure modes were the same.

This study suggests that the technique of measuring reradiated emissions may be used to quantify the degree of interaction between a digital EUT and external interference at field levels well below those which cause a observable functional failure of the equipment. It is therefore able to probe the interference regime in which dynamic failures of the EUT could occur, although it is not able to detect such failures directly. The evaluation of the reradiated spectra could also provide information about which part(s) of a complex system has caused a failure and therefore could be useful as a diagnostic tool.

REFERENCES

- [1] D. J. Kenneally, D. S. Koellen, and S. Epstein, "RF upset susceptibility of CMOS and low power Schottky D-type flip-flops," in *Proc. IEEE Int. Symp. Electromagnetic Compatibility*, Denver, CO, May 1989, pp. 190–195.
- [2] J. F. Chappel and S. Zaky, "EMI effects and timing design for increased reliability in digital systems," *IEEE Trans. Circuits Syst. I*, vol. 44, pp. 130–142, Feb. 1997.
- [3] M. P. Robinson, T. M. Benson, C. Christopoulos, J. Dawson, M. D. Ganley, A. C. Marvin, S. J. Porter, D. W. P. Thomas, and J. D. Turner, "Effect of component choice on the immunity of digital circuits," in *Proc. Int. Symp. Electromagnetic Compatibility (ROMA'96)*, Rome, Italy, Sept. 1996, pp. 233–236.
- [4] J.-J. Laurin and S. G. Zaky, "On the prediction of digital circuit susceptibility to radiated EMI," *IEEE Trans. Electromagn. Compat.*, vol. 37, pp. 528–535, Nov. 1995.
- [5] S. Wendsche and E. Habiger, "Using reinforcement learning methods for effective EMC immunity testing of computerised equipment," in *Proc. Int. Symp. Electromagnetic Compatibility (ROMA'96)*, Rome, Italy, Sept. 1996, pp. 221–226.
- [6] R. Vick and E. Habiger, "The dependence of the immunity of digital equipment on the hardware and software structure," in *Proc. Int. Symp. Electromagnetic Compatibility*, Beijing, China, May 1997, pp. 383–386.
- [7] T. Konefal and A. C. Marvin, "Prediction and measurement of EMC radiated immunity problems in interconnected digital systems," *Proc. IEE Sci. Meas. Technol.*, vol. 141, no. 6, pp. 464–470, 1994.
- [8] —, "UHF inter-modulation product prediction in digital systems using SPICE: the need for nonlinear macromodels," *Proc. IEE Sci. Meas. Technol.*, vol. 143, no. 5, pp. 313–318, 1996.
- [9] M. P. Robinson, K. Kischer, I. D. Flintoft, and A. C. Marvin, "A simple model of EMI-induced timing jitter in digital circuits, its statistical distribution and its effect on circuit performance," *IEEE Trans. Electromagn. Compat.*, vol. 45, pp. 513–519, Aug. 2003.



Ian D. Flintoft (M'00) received the B.Sc. and Ph.D. degrees in physics from the University of Manchester, Manchester, U.K., in 1988 and 1994, respectively.

He became a Research Fellow in Applied Electromagnetics at the University of York, York, U.K., in 1996. He is currently active in a number of areas of research including computational electromagnetics, immunity of digital systems, electromagnetic compatibility (EMC) in complex and distributed systems and EMC aspects of telecommunication systems.



Andrew C. Marvin (M'85) received the M.Eng. and Ph.D degrees from the University of Sheffield, Sheffield, U.K., in 1974 and 1979, respectively.

He is Professor of Applied Electromagnetics at the University of York, York, U.K. and Technical Director of York EMC Services Ltd. His research interests include electromagnetic compatibility (EMC) measurement techniques, EMC shielding measurements, EMC antenna design, and equipment design techniques for EMC.

Dr. Marvin is currently Chairman of the Management Committee of COST Action 286 (EMC in Diffused Communications Systems), U.K. delegate to URSI panel A, and an Associate Editor of the *IEEE TRANSACTION ON ELECTROMAGNETIC COMPATIBILITY*. He is a Chartered Engineer in the U.K. and a Member of the Institution for Electrical and Electronic Engineers, U.K.



Martin P. Robinson received the of B.A. and M.A. degrees from the University of Cambridge, Cambridge, U.K., in 1986 and 1990, respectively, the M.Sc. degree in medical physics from the University of Aberdeen, Aberdeen, U.K., in 1990, and the Ph.D. degree in dielectric imaging from the University of Bristol, Bristol, U.K., in 1994

He worked for two years at the National Physical Laboratory, Teddington, U.K., and for three years at Bristol Oncology Centre, Bristol, U.K. He joined the University of York, York, U.K. in 1993, where he is currently a Lecturer in Electronics. His research interests include design for electromagnetic compatibility (EMC), dielectric measurements, and the interaction of electromagnetic radiation with biological tissues.

Katharina Fischer received the Vordiplom in electronics from the University of York, York, U.K., in 2001 and is working toward the degree from the University of Hanover, Hanover Germany.

Andrew J. Rowell received the M.A. degree from University of Cambridge, Cambridge, U.K., and the M.Sc. degree in electromagnetic compatibility (EMC) from the University of York, York, U.K.

He worked at VSEL (now BAE Systems), Barrow-in-Furness, U.K., for ten years in electronic design, system integration and electromagnetic compatibility (EMC) testing activities. He spent a further period at Tunstall Electronics, Doncaster, U.K., as an EMC Specialist before joining York EMC Services, York, U.K., where his is now a Senior EMC Engineer, working on EMC testing and measurement projects, including research on EMC measurements at frequencies above 1 GHz.